



HAL
open science

The Atmospheric Drivers of the Major Saharan Dust Storm in June 2020

Diana Francis, Ricardo Fonseca, Narendra Nelli, Juan Cuesta, Michael Weston, Amato Evan, Marouane Temimi

► **To cite this version:**

Diana Francis, Ricardo Fonseca, Narendra Nelli, Juan Cuesta, Michael Weston, et al.. The Atmospheric Drivers of the Major Saharan Dust Storm in June 2020. *Geophysical Research Letters*, 2020, 47 (24), 10.1029/2020GL090102 . hal-04278557

HAL Id: hal-04278557

<https://cnrs.hal.science/hal-04278557>

Submitted on 10 Nov 2023

HAL is a multi-disciplinary open access archive for the deposit and dissemination of scientific research documents, whether they are published or not. The documents may come from teaching and research institutions in France or abroad, or from public or private research centers.

L'archive ouverte pluridisciplinaire **HAL**, est destinée au dépôt et à la diffusion de documents scientifiques de niveau recherche, publiés ou non, émanant des établissements d'enseignement et de recherche français ou étrangers, des laboratoires publics ou privés.

Geophysical Research Letters

RESEARCH LETTER

10.1029/2020GL090102

Key Points:

- The dust storm was triggered by the development of a subtropical high off the coast of West Africa embedded in a circumglobal wavetrain
- The stationary subtropical high increased the north-south pressure gradient over the Sahara and generated sustained strong northeasterlies
- The anticyclonic circulation associated with the high intensified the African Easterly Jet favoring a rapid westward transport of the dust plumes

Supporting Information:

- Supporting Information S1

Correspondence to:

D. Francis,
diana.francis@ku.ac.ae

Citation:

Francis, D., Fonseca, R., Nelli, N., Cuesta, J., Weston, M., Evan, A., & Temimi, M. (2020). The atmospheric drivers of the major Saharan dust storm in June 2020. *Geophysical Research Letters*, 47, e2020GL090102. <https://doi.org/10.1029/2020GL090102>

Received 29 JUL 2020
Accepted 16 NOV 2020

© 2020. The Authors.

This is an open access article under the terms of the Creative Commons Attribution-NonCommercial-NoDerivs License, which permits use and distribution in any medium, provided the original work is properly cited, the use is non-commercial and no modifications or adaptations are made.

The Atmospheric Drivers of the Major Saharan Dust Storm in June 2020

Diana Francis¹, Ricardo Fonseca¹, Narendra Nelli¹, Juan Cuesta², Michael Weston¹, Amato Evan³, and Marouane Temimi⁴

¹Environmental and Geophysical Sciences (ENGEOS) Laboratory, Khalifa University of Science and Technology, Abu Dhabi, UAE, ²Laboratoire Interuniversitaire des Systèmes Atmosphériques, CNRS and Université Paris-Est Créteil Val de Marne, Créteil, France, ³Scripps Institution of Oceanography, University of California, San Diego, La Jolla, CA, USA, ⁴Department of Civil, Environmental, and Ocean Engineering (CEOE), Stevens Institute of Technology, Hoboken, NJ, USA

Abstract This study investigates the atmospheric dynamics of the major dust storm that occurred in June 2020 over the Sahara and during which dust clouds associated with the highest-on-record aerosol optical depths were transported toward the America. An anomalous atmospheric circulation pattern in the mid-latitudes, linked to a circumglobal wavetrain, resulted in the development of a subtropical high-pressure system to the west of the Saharan heat low. This created a pressure dipole and generated anomalously strong northeasterlies over the Sahara, which caused continuous dust emissions over 4 days. Occurring along the northern fringes of the intertropical discontinuity, the dust was transported to higher altitudes (6 km) by the strong updraft in this region. This injected the dust at the African Easterly Jet (AEJ) altitudes and favored a rapid westward long-range transport. The AEJ was also anomalously strong, being strengthened by the anticyclonic circulation associated with the anomalous high.

Plain Language Summary Dust is an important constituent of the Earth's atmosphere, with a wide range of impacts ranging from human health to effects on climate. In June 2020, massive amounts of dust were lifted from the Sahara, the major dust source region in the world, and transported all the way into the Americas across the tropical Atlantic Ocean. This event was caused by the development of a subtropical high-pressure system over northwest Africa which resulted in sustained strong northeasterlies over the Sahara generating continuous dust emissions for 4 days. Due to the strong low-level convergence along the intertropical discontinuity region, the dust was lifted to roughly 5–6 km above the surface, and then transported westward by the stronger mid-atmospheric winds ($>20 \text{ m s}^{-1}$). At Cape Verde and over large swaths of the Atlantic Ocean, the amount of dust suspended in the atmosphere was associated with the largest aerosol optical depths on record.

1. Introduction

Mineral dust is the most common aerosol type on Earth and it has a wide range of impacts ranging from effects on human health (de Longueville et al., 2013), on the local and regional climate (Schepanski, 2008; Weston et al., 2020) and on tropical cyclones (Evan et al., 2006; Pan et al., 2018). The Sahara Desert in North Africa is widely recognized as the major source of mineral dust aerosols in the world (Middleton & Goudie, 2001). Therefore, an understanding of the mechanisms responsible for dust lifting in the Sahara and its long-range transport, in particular in the summer when dust events are more frequent in the area (Engelstaedter & Washington, 2007; Knippertz & Todd, 2012), is crucial.

The predominant large-scale summertime atmospheric circulation feature in North Africa is the Saharan heat low (SHL). The SHL is a thermal low, developing from the strong heating of the surface by the Sun, and subsequent warming of the atmosphere through sensible heat fluxes (Almirew et al., 2018; Lavaysse et al., 2009). As a result of the strong surface heating, rather deep boundary layers, which can extend to more than 5 km above the surface (Flamant et al., 2007; Knippertz et al., 2009), arise during daytime. The meridional temperature gradient between the cooler and moister air over the Gulf of Guinea (the monsoon flow) and the hot air over the inland desert, through thermal wind balance, give rise to an easterly jet, denoted as the African Easterly Jet (AEJ; Thorncroft & Blackburn, 1999). The AEJ, which is both barotropically and

baroclinically unstable (Hsieh & Cook, 2008), peaks at 700 hPa (roughly 3 km above the surface) around 10°N–15°N. It plays an important role in modulating dust storms in the region and in the dust transport into the Atlantic Ocean. For example, Bou Karam et al. (2014) reported on a synoptic-scale dust event triggered by a cold pool that formed from a mesoscale convective system over the Sahara. This system developed as part of an exceptional northward surge of the monsoon, and its expansion as a density current lifted roughly 2×10^6 tons of dust from the Sahara Desert. As the dust reached the level of the AEJ owing to the deep boundary layers in the region (von Engel n & Teixeira, 2013), it was advected westwards into the Caribbean Sea, where locally unusual high amounts of dust were recorded. Such long-range transport of Saharan dust has been reported before (e.g., Doherty et al., 2008; Grob et al., 2015; Prospero & Lamb, 2003), and is tightly linked with the large-scale meteorology in North Africa. In particular, Rodriguez et al. (2015) discusses a dipole over western North Africa, characterized by a ridge over the subtropical Sahara, and a trough over tropical North Africa. It is denoted as the North African Dipole (NAFD), and its strength is measured using the NAFD index (NAFDI). Positive values of NAFDI correspond to a positive meridional pressure gradient over the Sahara (i.e., both features are stronger than the respective climatological means), with the resulting low-level easterlies over the desert favoring dust emission and subsequent export. The NAFD has been mentioned in subsequent publications such as Cuevas et al. (2017) and Schepanski et al. (2017), with high NAFDI values linked with high aerosol optical depths over West Africa and increased dust export into the Atlantic Ocean.

On top of the thermodynamic forcing, which gives rise to deep boundary layers that help to lift dust to a few kilometers above the surface, dynamical forcing can also contribute to dust lifting. At the interface where the hot and dry air from the desert blowing from a northerly direction meets the southerly cooler and moist air from the Gulf of Guinea, labeled as the intertropical discontinuity (ITD; Pospichal et al., 2010), the low-level wind convergence is balanced by vertical ascent. As highlighted in Bou Karam et al. (2008, 2009a), and in particular in June and July when the ITD sits over the Sahel, dust can be lifted several kilometers upwards, and then advected by the strong AEJ winds. Moreover, the presence of high terrain and associated impact on the atmospheric flow (i.e., orographic blocking and flow splitting), aids in the development of dry cyclones and subsequently impacts dust lifting (Bou Karam et al., 2009b, 2010). Synoptic-scale disturbances such as African easterly waves also modulate dust emissions in the Sahara Desert in the warm season (Knippertz & Todd, 2010). In the cold and transition seasons, on the other hand, dust storms are usually triggered by mid-latitude weather disturbances, in particular cut-off lows that drift southeastwards into northwestern Africa (D. Francis et al., 2018, 2019). At more local-scales, dust is lifted by different mechanisms such as (i) downward mixing of momentum from nighttime low-level jets after sunrise when the boundary layer deepens (e.g., Allen & Washington, 2014; Caton Harisson et al., 2019), (ii) convective downdrafts associated with deep convective events (e.g., Heinold et al., 2013), and (iii) dust devils that occur during daytime arising from the strong heating of the surface by the Sun (e.g., Knippertz & Todd, 2012). As noted by Schepanski et al. (2009), the combination of the referred local-scale forcing with that of the large-scales accounts for much of the variability of dust emissions on diurnal time-scales.

While the near-surface winds associated with the presence of an anomalous trough or ridge over the Sahara can lead to dust lifting (Tulet et al., 2008), this weather feature is typically not isolated in nature but constitutes part of a large-scale pattern of anomalies. Ding and Wang (2005) reported on a circumglobal teleconnection zonal wavenumber 5 pattern, which prevails in the northern hemisphere in the summer season, and is driven by the interaction between the subtropical jet stream and the Indian summer monsoon. A circumglobal wavetrain that persists for a considerable period of time can lead to extreme weather episodes at regional scale, as regions predominantly under the influence of a ridge will experience rather dry weather conditions, while the prevalence of low pressure systems may lead to flooding. This has been observed, for example, in summer 2007 (Blackburn et al., 2008) and summer 2008 (Kornhuber et al., 2019), when a wavenumber 7 wavetrain persisted in the northern hemisphere.

In this study, the mechanisms behind the 14–19 June, 2020 dust event, a record breaking event that led to the dustier atmospheric conditions in the tropical Atlantic since records began in 2002, is analyzed. Despite being a ubiquitous feature over the Sahara, intense dust storms comparable to the one in June 2020 remain unpredictable and their underlying mechanisms are still not fully understood. As such, the central goal of

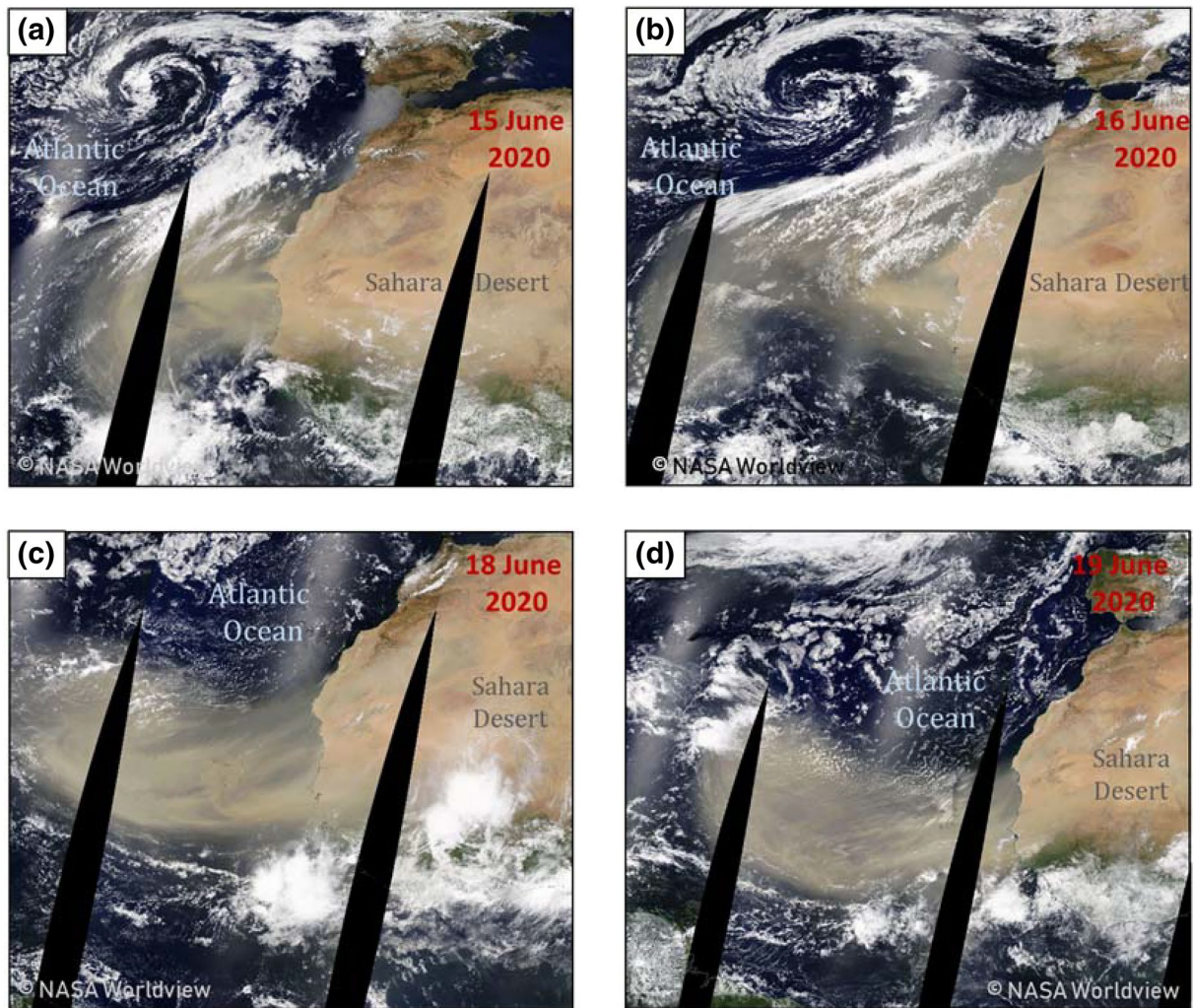


Figure 1. MODIS visible imagery on (a) 15, (b) 16, (c) 18, and (d) 19 June 2020 over western Africa and the northern tropical Atlantic Ocean. Clouds are in white and the dust is in yellow. Note the extensive dust layer originating from the Sahara Desert on June 15, 2020 that by June 19, 2020 covers a wide area over the surrounding Atlantic Ocean. Image credits NASA Worldview.

this work is to identify the processes responsible for the lifting and transport of the dust in this extreme event and their link to the large-scale circulation.

This paper is structured as follows. In Section 2, the synoptic conditions present during the dust event are analyzed, with the mechanisms responsible for the initiation of the event, and the subsequent transport of dust into the tropical Atlantic Ocean, discussed in Section 3. In Section 4, the characteristics of the dust storm are presented, using both satellite products and in situ measurements. The conclusions of the study are outlined in Section 5.

2. Synoptic Conditions

A synoptic-scale dust storm occurred in mid-June over the tropical Atlantic Ocean. Dust clouds covering several degrees in latitudes and longitudes can be seen in the visible satellite images from the Moderate Resolution Imaging Spectroradiometer (MODIS; Y. J. Kaufman et al., 1997, Y. Kaufman et al., 2002) on 15, 16, 18 and 19 June, 2020 (Figure 1). In addition to the dust clouds, a cut-off low is present to the northwest of Africa, with the cyclonic circulation and associated cloud pattern clearly seen in the satellite images. A

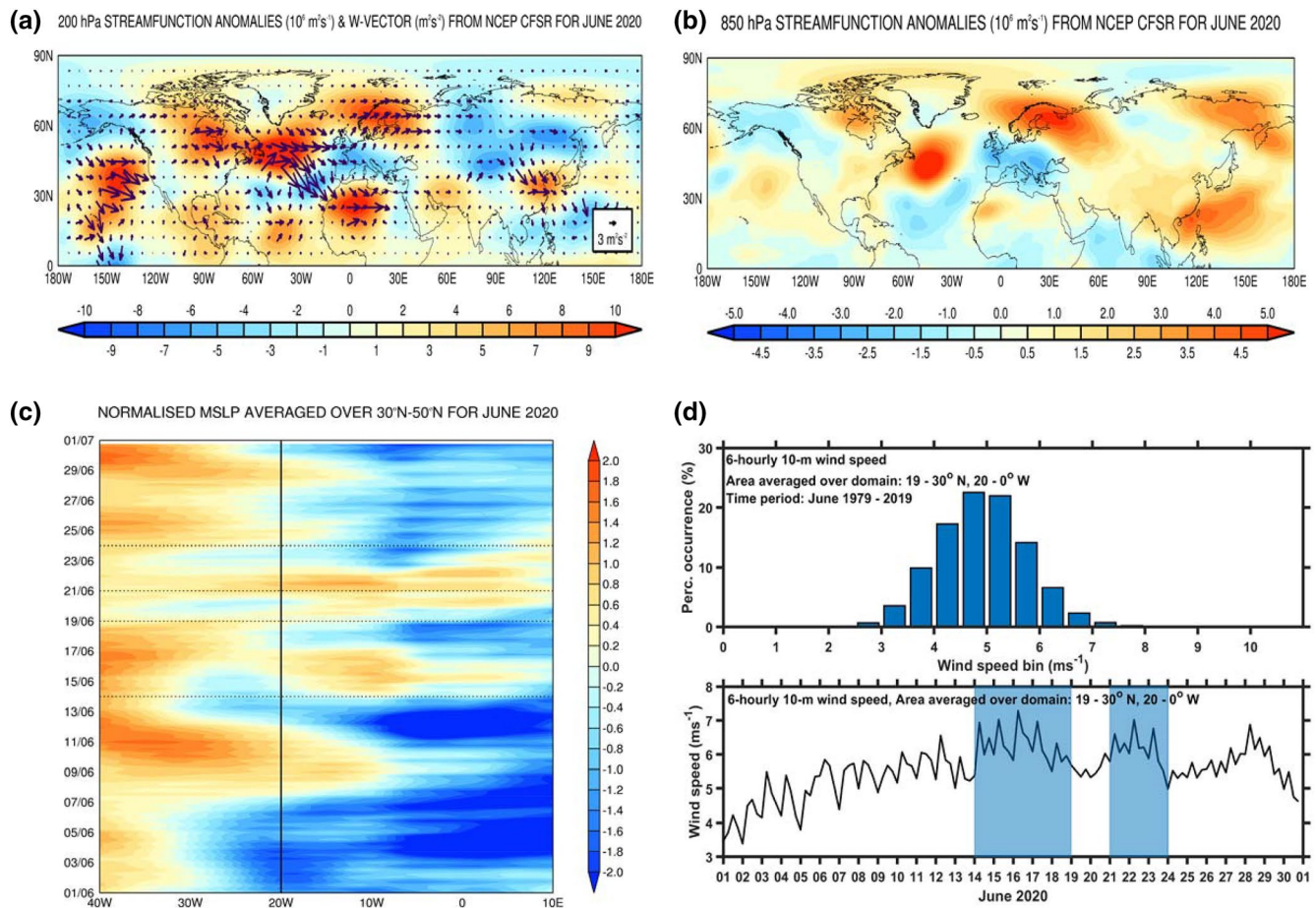


Figure 2. (a) 200 hPa and (b) 850 hPa stream function anomalies ($10^6 \text{ m}^2 \text{ s}^{-1}$) from the 1991 to 2020 NCEP CFSR climatology averaged over June 2020 for the northern hemisphere. In (a), the horizontal component of the Rossby wave activity flux, as defined by Takaya and Nakamura's (2001) W-vector ($\text{m}^2 \text{ s}^{-2}$), is plotted as arrows. (c) Hovmöller plot of 6-hourly MSLP anomalies normalized by the climatological standard deviation, averaged over 30°N to 50°N from 40°W to 10°E. The solid black line denotes the longitude of the West African coastline. The dotted black lines give the periods of intense dust storms. (d) The top panel shows a histogram of 6-hourly 10-m wind speed averaged over 19°N–30°N and 20°W–0°W for the period 1979–2019, while the bottom panel shows the 10-m wind speed observed during June 2020 for the same domain. The periods 14–19 June and 21–24 June are shaded in light blue.

plume of dust between this feature and the Intertropical Convergence Zone further south is clearly visible on 15 June, with the dust advected westwards into the tropical Atlantic Ocean on 18 and 19 June.

In this section, the large-scale atmospheric conditions in June 2020, and in particular during the 14–19 June, 2020 Saharan dust storm, are discussed. In order to give an overview of the upper- and lower-level circulation anomalies, Figures 2a and 2b show the 200 and 850 hPa streamfunction anomalies from the National Centers for Environmental Prediction (NCEP) Climate Forecast System Reanalysis (CFSR; Saha et al., 2010) averaged over June 2020 for the northern hemisphere, respectively. A similar analysis using MERRA-2 reanalysis data (Gelaro et al., 2017) gave identical results (not shown) to the ones discussed here.

A wavetrain is seen over the North Atlantic Ocean, with a branch extending from northeastern North America to northern Africa, and another over northern Europe into Siberia. The pattern of anomalies over Europe and northern Africa, with a low over western Europe and a high over northwestern Africa, suggests a southward displacement of the jet stream around 20°W. This wavetrain appears to be linked to a similar jet displacement over the Pacific Ocean, indicating the presence of a large-scale pattern of anomalies across the whole hemisphere that persisted for the month of June. This circumglobal wavetrain was also responsible for the unusually dry and hot weather over northeastern Siberia, and may have played a role in the wet conditions in parts of China running into July. A comparison with Figure 2b shows that the wavetrain

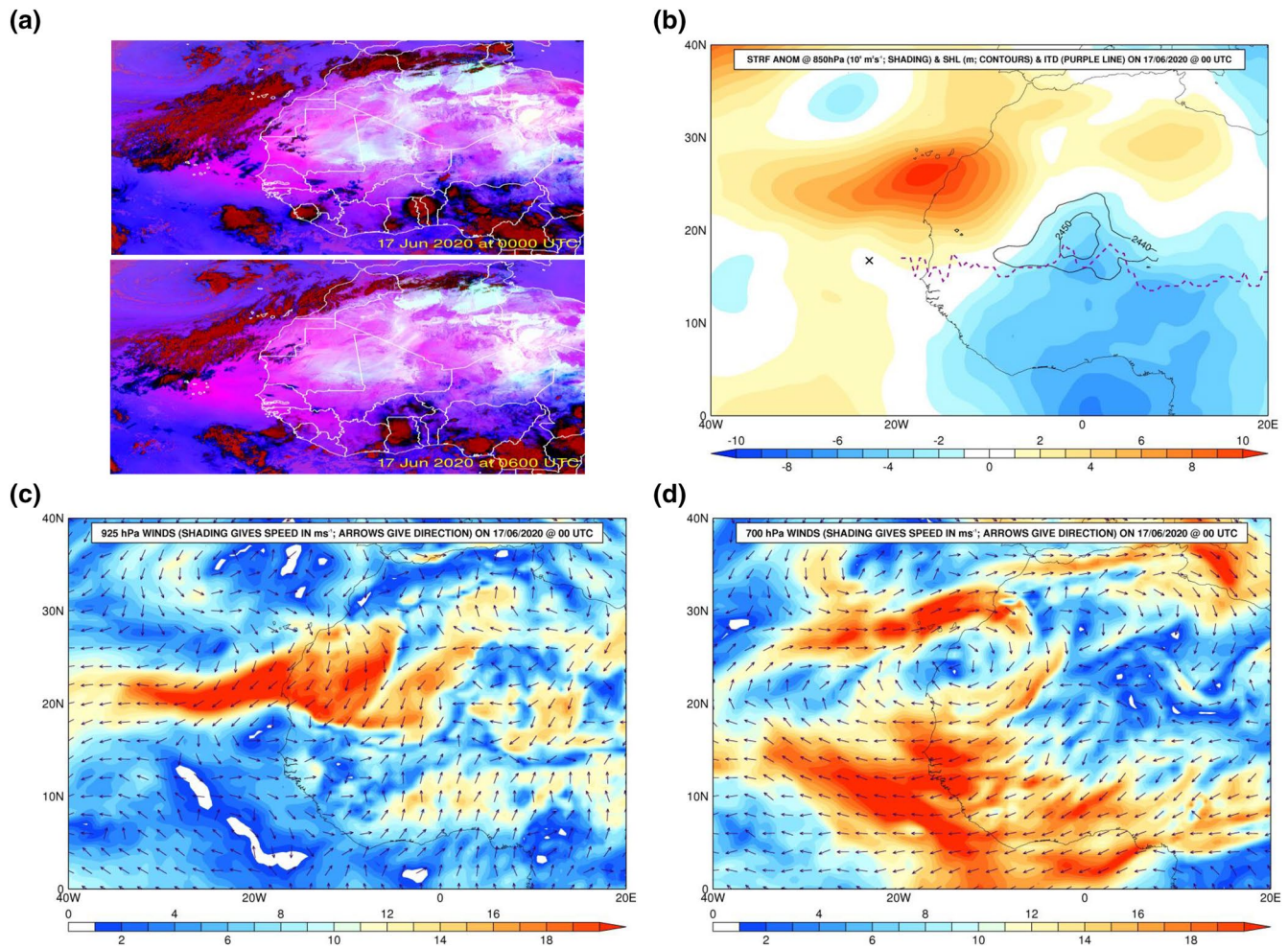


Figure 3. (a) SEVIRI RGB dust product on 17 June at 00 and 06 UTC and at 00 UTC. (b) Stream function anomalies with respect to 1991–2020 NCEP CFSR climatology at 850 hPa ($10^6 \text{ m}^2 \text{ s}^{-1}$; shading), SHL (m; two solid contours) and ITD (dashed line), (c) 925 hPa horizontal wind speed (m s^{-1} ; shading) and direction (arrows), and (d) same as (c) but at 700 hPa. In (a), clouds are shaded in orange or brown, dust is given in magenta or pink, sandy regions are shaded in white, and dry land is highlighted in pale blue. The cross in panel (b) denotes the location of the AERONET station for which in situ AOD measurements are given in Figure 5. AOD, aerosol optical depth.

is largely equivalent barotropic, with a baroclinic structure over southeast Asia (and the eastern tropical Indian Ocean) and the central Pacific Ocean, likely a response to the enhanced convective activity over the former and suppressed convection over the latter. These forcings may be related to the mature phase of a decaying El Niño event, where the heating anomaly over the tropical Indian Ocean plays the largest role in the atmospheric response (e.g., Xie et al., 2009). Tropical forcing is indeed a common origin of such persistent large-scale patterns (e.g., Behera et al., 2013).

An anomalous ridge at 850 hPa, centered around 7°W , can be seen over northwestern Africa (Figure 2b). In order to inspect its evolution during the month, Figure 2c shows the 6-hourly mean sea-level pressure (MSLP) anomalies, normalized by the climatological standard deviation, averaged over 30°N – 50°N from 40°W to 10°E . A stronger than normal thermal low over the Sahara and high pressure offshore were present throughout the month, with steep pressure gradient building over northwestern Africa during the few days preceding the two periods 15–19 and 21–24 June (Figure 2c). During these two periods, sustained record-high surface winds (Figure 2d) resulted from the strong pressure gradient formed by the anomalous ridge around 18°W and the monsoon trough to the south of it and the SHL to its southeast (Figure 3b). Even though the NAFDI was positive during this part of the event (15–17 June), the placement of the high pressure is very different from that in positive NAFDI events, where the ridge is over northern Algeria and

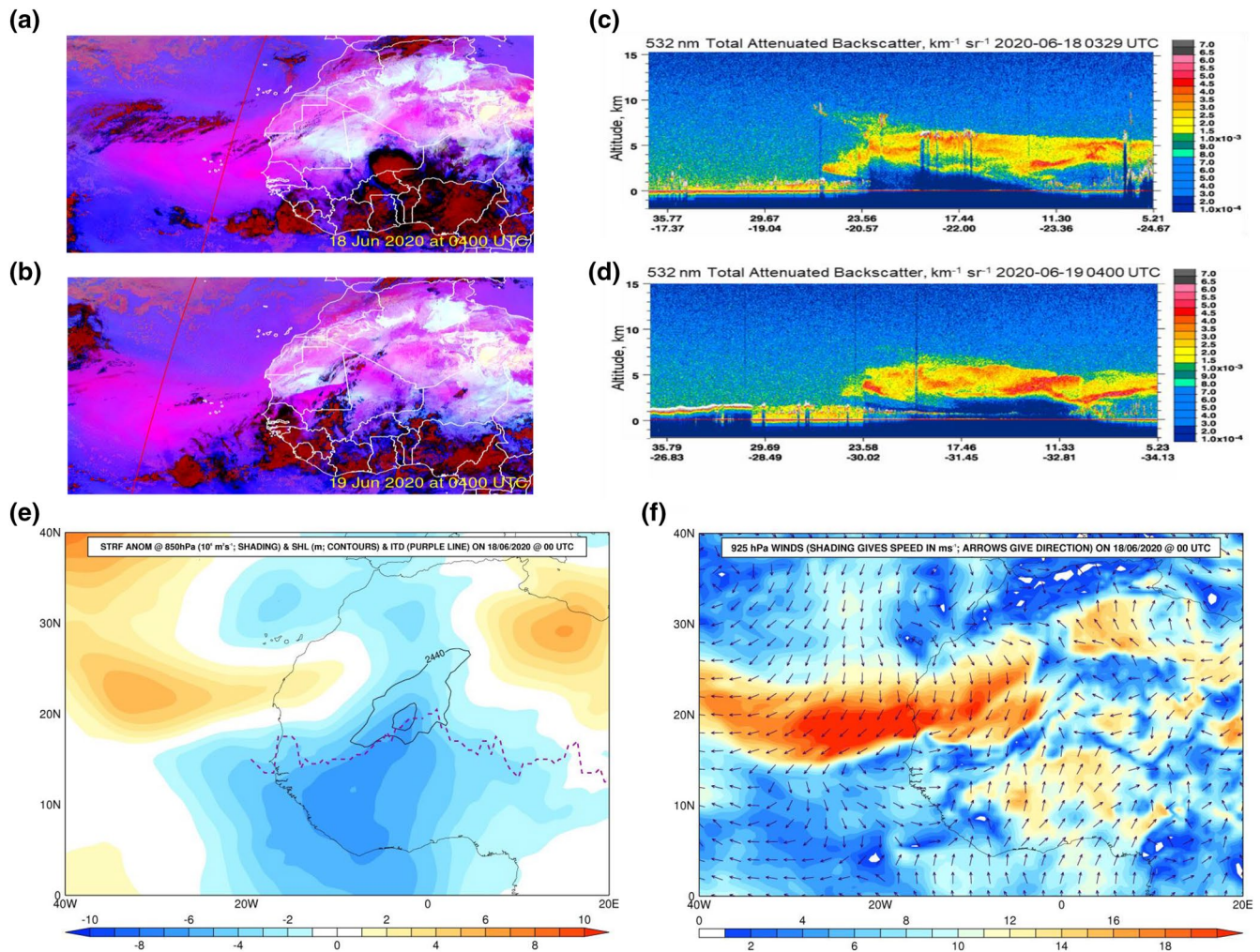


Figure 4. (a) SEVIRI RGB dust product on 18 June at 04 UTC, (b) same as (a) but on 19 June at 04 UTC. On SEVIRI images dust appears in pink colors. (c) CALIPSO 532 nm total attenuated backscatter coefficient ($\text{km}^{-1} \text{sr}^{-1}$) on June 18, 2020 at 03:29 UTC, whose track is given by the red solid line on (a). The dust appears in yellow and red in the CALIPSO observations. (d) Same as (c) but on 19 June at 04 UTC and along the track given by the red solid line on (b). On June 18, 2020 at 00 UTC, (e) stream function anomalies with respect to 1991–2020 NCEP CFSR climatology at 850 hPa ($10^6 \text{ m}^2 \text{ s}^{-1}$; shading), SHL (m; two solid contours) and ITD (dashed line), and (f) 925 hPa horizontal wind speed (m s^{-1} ; shading) and direction (arrows).

Morocco (see Figure 2 of Rodriguez et al., 2015). Hence, the NAFDI captured part of the high that is located over land, but the majority of it was over the ocean, as seen in Figures 2c and 3b. The area-averaged 10-m wind speed over northwestern Africa was on the higher side of the climatological values, with instantaneous surface winds peaking at 20 m s^{-1} (Figures 3c, 4f, S1d, and S2d). This analysis indicates that the observed dust storm from 14 to 19 June 2020 was triggered by the atmospheric circulation associated with a ridge centered off the coast of northwestern Africa that itself was part of a large-scale pattern of anomalies.

3. Dust Emission and Transport

In order to better understand the development of the dust storm, Figures 3 and 4 show the atmospheric variables on 17 and 18 June in combination with the horizontal and vertical distribution of dust aerosols. These were inferred respectively from the false-color red-green-blue (RGB, Banks et al., 2019) images from the Spinning Enhanced Visible and Infrared Imager (SEVIRI; Schmetz et al., 2002) and from the total attenuated backscatter profile derived from the Cloud-Aerosol Lidar and Infrared Pathfinder Satellite Observation (CALIPSO; Winker et al., 2003) satellite. Similar plots for 15, 16, 19, and 20 June are given in Figures S1–S4.

The SHL and the ITD on Figures 3b and 4e were identified following Lavaysse et al. (2009), where the SHL is the region with the highest 10% values of the cumulative distribution of the 925 hPa minus 700 hPa thickness at 06 UTC in the domain 20°W–30°E and 0°N–40°N. The position of the ITD is given by the location of the lowest 925 hPa geopotential height between the equator and 28°N.

The dust storm started on 14 June and was continuous till 19 June, when it dissipated after the merging of the ridge and the cut-off low with the general circulation (i.e., Figure 4e). On 17 June at 00 UTC, a widespread dusty area was observed extending from western Africa to the eastern tropical Atlantic Ocean, denoted by the pink shading in Figure 3a. The dust was lifted by the northwesterlies turning northeasterlies over northwestern Africa, associated with the anomalous high over northwest Africa and the resulting zonal pressure gradient between this high and the SHL located to its east (Figure 3b). In addition to the east-west pressure gradient (e.g., Figure S2b), the meridional pressure gradient between the high-pressure system and the monsoon trough helped to accelerate the winds toward the ITD. The placement of the high pressure system also helped to rapidly advect the dust away from the source region into the tropical Atlantic mostly around the 20°N latitude band (Figure 3d). Aiding the dust lifting is the presence of the ITD just to the south of the emission region (Figure 3b) as the strongest low-level northeasterly winds are typically observed just northward of this feature (Figure 3c). As the dust is lifted higher up in the atmosphere its westward transport is accelerated once it reaches 700 hPa (~3 km above ground level), the altitude of the AEJ that, at this time, had speeds in excess of 20 m s⁻¹ just south of 20°N, as seen in Figure 3d. A cut-off low was also present to the west of the anomalous high-pressure system (Figures 1a, 1b, and 3b). The cyclonic circulation associated with this cut-off low may have helped in intensifying the anticyclonic winds around the high-pressure system seen at 700 hPa (Figure 3d), which in turn favored a strengthening of the AEJ by directing into it strong northeasterlies (Figure 3d).

A day later, on June 18, 2020, the dust plume reached the central tropical Atlantic Ocean, as highlighted by the vast pink region in Figure 4a, and as is evident in the visible imagery (Figure 1c). Figure 4c shows a backscatter vertical profile as measured by CALIPSO on June 18, 2020 to the west of the African coast. In the pink region in Figure 4a, dust reaches very high altitudes, in excess of 6 km in the dark pink area just off the coast of Senegal, where the ITD was located at the time (Figure 4c). The dust cloud continued its westward propagation (Figure 4b) at the same altitudes as evidence in CALIPSO observations on June 19, 2020 (Figure 4d). The cut-off low to the north of the Canary Islands tracked northeastwards, and would later rejoin the mid-latitude jet stream, while the high-pressure system shifted southwestwards (Figure 4e). The zonal pressure gradient increased compared to the previous day (Figure 2c), with particularly strong northerly winds just offshore of the African coast and to the north of the ITD (Figure 4e). This, together with an equally strong AEJ (Figure 4f), helped to advect the dust further westwards, which continued to be lifted from the inland desert (Figures 1c, 1d, and 4a). Similar synoptic-scale conditions and associated dust emission and westward transport lasted during the 14–19 June period (Figures S1–S4). The large-scale pattern on 21–24 June resembled that of the positive phase of the NAFD (Figure S5), where a subtropical high over north Africa induced dust lifting and export of Saharan dust into the Atlantic Ocean (Rodriguez et al., 2015).

4. Characteristics of the Dust Storm

The westward transport of dust continued in the days following the initial burst of the dust clouds from the Sahara (Figures 5a, 5b, and S4), with the dust reaching North America later in the month (Figures 5a and 5b). CALIPSO observations through the dust cloud over the Atlantic Ocean show a thick dust layer between 3 and 7 km in altitudes covering several degrees in latitudes and longitudes (Figures 4c, 4d, and S4b). The three-dimensional distribution of dust derived from AEROIASI satellite (Cuesta et al., 2015, 2020) revealed a thick layer of dust along the northern side of the ITD extending from the surface to 5 km in altitudes on June 19, 2020 (Figure S4c) and a more detached layer from the surface on June 20, 2020 (Figure S4d) especially above the marine boundary layer.

In order to quantify the dust event, Figure S6 shows the aerosol optical depth (AOD), as measured by satellite over the eastern tropical Atlantic and Figure 5d shows the AOD observed at a weather station in Cape Verde islands (cross in Figure 3b), for the month of June. According to both, the June 2020 dust event was

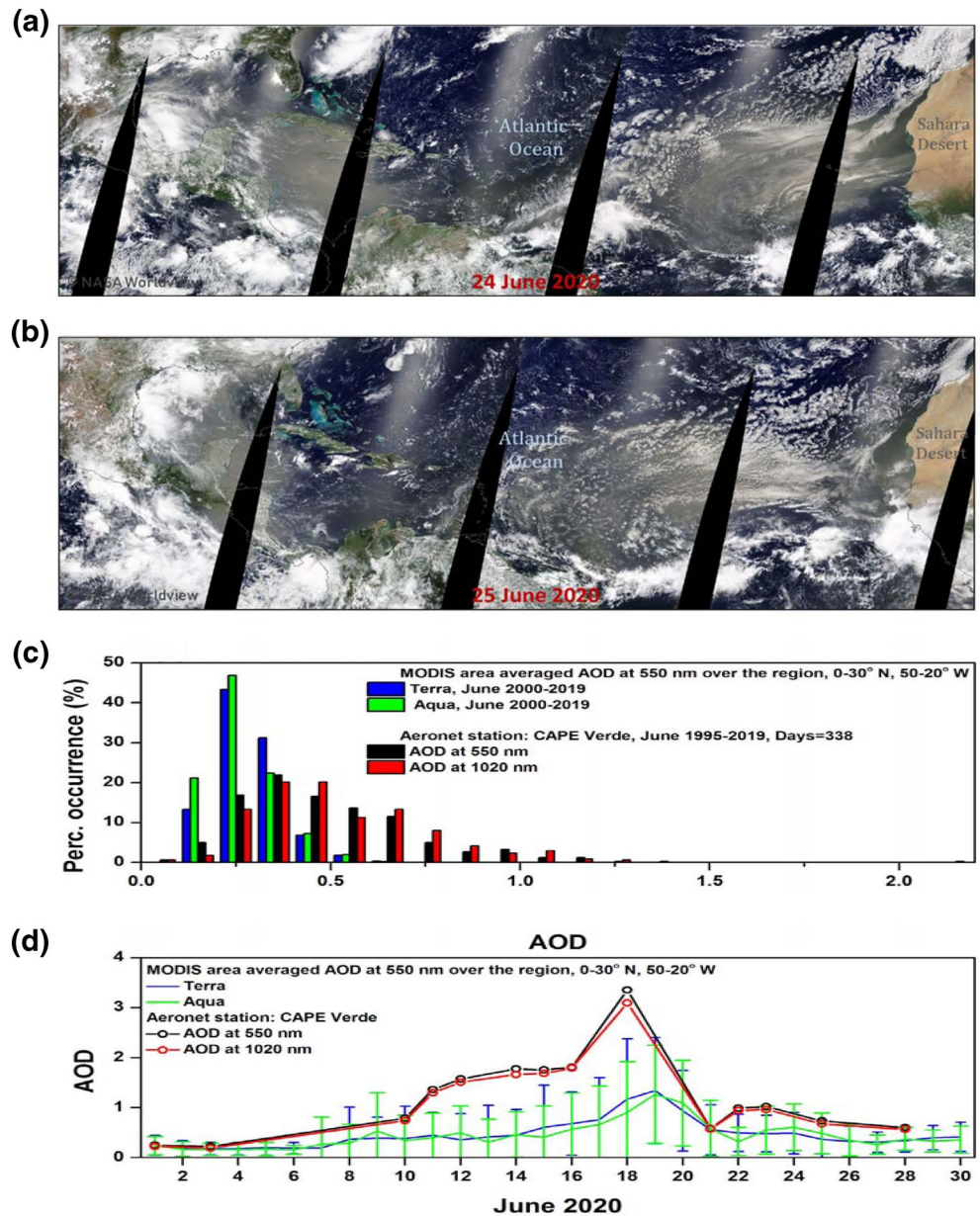


Figure 5. MODIS visible imagery on (a) 24 and (b) 25 June 2020 over the northern tropical Atlantic Ocean. Dust appears in yellow and clouds in white colors. Note the extensive dust layer that originated from the Sahara Desert on June 15, 2020 and that by June 25, 2020 reached Central America and parts of southern United States of America. An extensive dust cloud was present also on 24 and 25 June over the Atlantic Ocean and reached the Americas by the end of June 2020. Image credits NASA Worldview. (c) Histogram of daily AOD from MODIS (area-averaged over the region 0°N - 30°N and 50°W - 20°W) for all June months during the period 2000–2019 (blue is from Terra, MOD04_L2 product and green is from Aqua, MYD04_L2 product), and in situ measurements at the AERONET station in Cape Verde (16.733°N ; 22.935°W), also for all June months during the period 1995–2019 (black is AOD at 550 nm, and red at 1,020 nm). (d) Day-to-day variability in the satellite-derived AOD over the region 0°N - 30°N and 50°W - 20°W , and that measured at Cape Verde, during June 2020. The error bars in (d) denote one standard deviation away from the mean. AOD, aerosol optical depth.

historical by June standards. The range of area-averaged AODs in the climatological period of the MODIS' instrument onboard the Terra and Aqua satellites are 0.140–0.692 and 0.107–0.653, respectively. However, area-averaged AODs in excess of 1.26 were observed by the two satellites on June 19, 2020, with maximum values of 1.341 and 1.266, respectively. In fact, and as shown in Figure S6, local AOD values in excess of

3.5 were measured by both satellites in the eastern tropical Atlantic. At the AERONET station, the highest observed AOD from 1995 to 2019 was 2.207, but on June 18, 2020 a value of roughly 3.355 was measured, a ~52% increase from the previous maximum. The AOD gradually increased from 10 to 16 June, peaking on 18 June, when the dust plume was over the region (Figure 1c) followed by a significant drop to climatological values on June 21, 2020, in line with the advection of the dusty air mass westwards to the central Atlantic (Figures 1d and 4a). Worth mentioning that extreme values of AOD reaching 5 were measured at the AERONET station on June 17, 2020 (level 1.0, not shown) but were screened out as clouds in the level 1.5 used here (although the MODIS visible imagery did not show cloud presence over this station on that day). Although rather unusual, such high AOD values would not be unprecedented. For example, Solomos et al. (2018) and Kaskaoutis et al. (2019) observed AOD values in excess of 6 over the eastern Mediterranean during the record-breaking March 2018 dust event. Finally, it is worth mentioning that the use of MODIS observations represents the best option to address the objectives of this study, despite the uncertainties that this data set may contain associated with swath gaps, cloud cover, and algorithm deficiencies.

5. Conclusions

In this paper, the processes responsible for the June 14–19, 2020 historical Saharan dust storm (by June standards) are investigated using satellite-derived products and high-resolution reanalysis data. The event was triggered by record-high northeasterly near-surface winds, associated with (i) the development of a subtropical high-pressure system over northwestern Africa situated to the west of the SHL and (ii) the occurrence of an adjacent cut-off low to the west of the high-pressure system located over the Atlantic Ocean. These features were part of a circumglobal wavetrain that persisted across the whole northern hemisphere for most of June 2020.

The east-west pressure dipole over northwest Africa generated anomalous northeasterlies along the northern fringes of the ITD, a region characterized by strong horizontal convergence and updraft. This promoted the vertical transport of the uplifted dust to the AEJ altitudes, which was also strong during this event, being fueled by the anticyclonic circulation associated with the high-pressure. CALIPSO total attenuated backscatter profiles from an overpass just off the African coast showed that the dust plume reached altitudes of up to 8 km near the ITD. The dust was transported westward into the tropical Atlantic Ocean over the course of 4 days, and at the same altitudes, according to consecutive CALIPSO overpasses. Both the satellite-derived AOD over the eastern tropical Atlantic, and that measured in situ at a weather station in the Cape Verde islands just off the African coast, were record breaking in June 2020. For the latter, the 3.355 value measured on June 18, 2020 exceeded the previous highest value of 2.207 by more than a factor of 1.52, further highlighting the extreme nature of this event.

Several previous studies have shown that the high surface wind speeds that generate Saharan dust storms during the summer season are often associated with mesoscale processes such as convective downdrafts from monsoonal (Bou Karam et al., 2014; Flamant et al., 2007; Marsham et al., 2008) or orographically forced convection (e.g., Knippertz et al., 2007), turbulent mixing at the leading edge of the monsoon flow in the ITD region (Bou Karam et al., 2008), formation of dry cyclones in the ITD (Bou Karam et al., 2009a) and flow acceleration toward the SHL (Knippertz & Todd, 2012). Yet this exceptional event was triggered by an intensified anticyclonic system, which strengthened the northwesterly flow over the Western Sahara, which was surprising given that such dust producing mechanisms are typically associated with wintertime dust outbreaks in this region (Evan et al., 2006; Knippertz, 2014, and references therein). The cause of this persistent circumglobal circulation pattern that forced this anomalous anticyclonic circulation is not obvious. Interestingly, the wavetrain pattern in Figure 2a resembles that obtained by Balmaseda et al. (2010) and Petrie et al. (2015) in response to a reduced summertime Arctic sea-ice extent. As the Arctic sea-ice cover was rather low in June 2020, around the lowest on record in the period of satellite observations (1981–present), it may have contributed to the observed large-scale anomaly pattern. Thus, if such patterns become more common in a warmer world (J. A. Francis & Vavrus, 2012; Terink et al., 2013), it is plausible that these extreme dust outbreaks will increase in frequency in the future.

Saharan dust is known for its impact on inhibiting the development of tropical cyclones off the coast of Africa via radiative impacts (Evan et al., 2006). The findings of this work help to shed light on the atmospheric

processes responsible for extreme Saharan dust storms over the tropical Atlantic and their link to the large-scale circulation. These findings can aid in the prediction of similar events in the future and their impacts on the tropical cyclones' activity in summer. An investigation of the role of local-scale forcing mechanisms such as low-level jets on June 2020 dust events will be left to future work.

Conflict of Interest

The authors declare no conflicts of interest relevant to this study.

Data Availability Statement

All the data used in the present analysis are available here <https://zenodo.org/record/4164761#.X52s4fkzbiU>.

Acknowledgments

We would like to thank Bob Dattore from the University Corporation for Atmospheric Research for making the National Centers for Environmental Prediction Climate Forecast System Reanalysis data freely available online. We would also like to thank two anonymous reviewers for their detailed and insightful comments and suggestions, which helped to significantly improve the quality of the manuscript.

References

- Allen, C. J. T., & Washington, R. (2014). The low-level jet dust emission mechanism in the central Sahara: Observations from Bordj-Badji Mokhtar during the June 2011 Fennec Intensive Observation Period. *Journal of Geophysical Research: Atmospheres*, *119*, 2990–3015. <https://doi.org/10.1002/2013JD020594>
- Almirew, N. K., Todd, M. C., Ryder, C. L., Marsham, J. H., & Wang, Y. (2018). The early summertime Saharan heat low: Sensitivity of the radiation budget and atmospheric heating to water vapour and dust aerosol. *Atmospheric Chemistry and Physics*, *18*, 1241–1262. <https://doi.org/10.5194/acp-18-1241-2018>
- Balmaseda, M. A., Ferraini, L., Molteni, F., & Palmer, T. N. (2010). Impact of 2007 and 2008 Arctic ice anomalies on the atmospheric circulation: Implications for long-range predictions. *Quarterly Journal of the Royal Meteorological Society*, *136*, 1655–1664. <https://doi.org/10.1002/qj.661>
- Banks, J. R., Hunerbein, A., Heinold, B., Brindley, H. E., Deneke, H., & Schepanski, K. (2019). The sensitivity of the colour of dust in MSG-SEVIRI Desert Dust infrared composite imagery to surface and atmospheric conditions. *Atmospheric Chemistry and Physics*, *19*, 6893–6911. <https://doi.org/10.5194/acp-19-6893-2019>
- Behera, S., Ratnam, J. V., Masumoto, Y., & Yamagata, T. (2013). Origin of extreme summers in Europe: The Indo-Pacific connection. *Climate Dynamics*, *41*, 663–676. <https://doi.org/10.1007/s00382-012-1524-8>
- Blackburn, M., Methven, J., & Roberts, N. (2008). Large-scale context for the UK floods in summer 2007. *Weather*, *63*, 280–288. <https://doi.org/10.1002/wea.322>
- Bou Karam, D., Flamant, C., Knippertz, P., Reitebuch, O., Pelon, J., Chong, M., & Dabas, A. (2008). Dust emissions over the Sahel associated with the West African monsoon intertropical discontinuity region: A representative case-study. *Quarterly Journal of the Royal Meteorological Society*, *134*, 621–634. <https://doi.org/10.1002/qj.244>
- Bou Karam, D., Flamant, C., Tulet, P., Chaboureaud, J.-P., Dabas, A., & Todd, M. C. (2009a). Estimate of Sahelian dust emissions in the intertropical discontinuity region of the West African Monsoon. *Journal of Geophysical Research*, *114*, D13106. <https://doi.org/10.1029/2008JD011444>
- Bou Karam, D., Flamant, C., Tulet, P., Todd, M. C., Pelon, J., & Williams, E. (2009b). Dry cyclogenesis and dust mobilization in the intertropical discontinuity of the West African Monsoon: A case study. *Journal of Geophysical Research*, *114*, D05115. <https://doi.org/10.1029/2008JD010952>
- Bou Karam, D., Flamant, C., Cuesta, J., Pelon, J., & Williams, E. (2010). Dust emission and transport associated with a Saharan depression: February 2007 case. *Journal of Geophysical Research*, *115*, D00H27. <https://doi.org/10.1029/2009JD012390>
- Bou Karam, D., Williams, E., Janiga, M., Flamant, C., McGraw-Herdeg, M., Cuesta, J., et al. (2014). Synoptic-scale dust emissions over the Sahara Desert initiated by a moist convective cold pool in early August 2006. *Quarterly Journal of the Royal Meteorological Society*, *140*, 2591–2607. <https://doi.org/10.1002/qj.2326>
- Caton Harrison, T., Washington, R., & Engelstaedter, S. (2019). A 14-year climatology of Saharan dust emission mechanisms inferred from automatically tracked plumes. *Journal of Geophysical Research: Atmospheres*, *124*, 9665–9690. <https://doi.org/10.1029/2019JD030291>
- Cuesta, J., Eremenko, M., Flamant, C., Dufour, G., Laurent, B., Bergametti, G., et al. (2015). Three-dimensional distribution of a major desert dust outbreak over East Asia in March 2008 derived from IASI satellite observations. *Journal of Geophysical Research: Atmospheres*, *120*, 7099–7127. <https://doi.org/10.1002/2014JD022406>
- Cuesta, J., Flamant, C., Gaetani, M., Knippertz, P., Fink, A.H., Chazette, P., et al. (2020). Three-dimensional pathways of dust over the Sahara during summertime 2011 as revealed by new IASI observations. *Quarterly Journal of the Royal Meteorological Society*, *146*, 2731–2755. <https://doi.org/10.1002/qj.3814>
- Cuevas, E., Gomez-Pelaez, A. J., Rodriguez, S., Terradellas, E., Basart, S., Garcia, R. D., et al. (2017). The pulsating nature of large-scale Saharan dust transport as a result of interplays between mid-latitude Rossby waves and the North African Dipole Intensity. *Atmospheric Environment*, *167*, 586–602. <https://doi.org/10.1016/j.atmosenv.2017.08.059>
- de Longueville, F., Ozer, P., Doumbia, S., & Henry, S. (2013). Desert dust impacts on human health: An alarming worldwide reality and a need for studies in West Africa. *International Journal of Biometeorology*, *57*, 1–19. <https://doi.org/10.1007/s00484-012-0541-y>
- Ding, Q., & Wang, B. (2005). Circumglobal teleconnection in the northern hemisphere summer. *Journal of Climate*, *18*, 3483–3505. <https://doi.org/10.1175/JCLI3473.1>
- Doherty, O. M., Riemer, N., & Hameed, S. (2008). Saharan mineral dust transport into the Caribbean: Observed atmospheric controls and trends. *Journal of Geophysical Research*, *113*, D07211. <https://doi.org/10.1029/2007JD009171>
- Engelstaedter, S., & Washington, R. (2007). Atmospheric controls on the annual cycle of North African dust. *Journal of Geophysical Research*, *112*, D03103. <https://doi.org/10.1029/2006JD007195>
- Evan, A. T., Dunion, J., Foley, J. A., Heidinger, A. K., & Velden, C. S. (2006). New evidence for a relationship between Atlantic tropical cyclone activity and African dust outbreaks. *Geophysical Research Letters*, *33*(19), L19813. <https://doi.org/10.1029/2006gl026408>

- Flamant, C., Chaboureaud, J.-P., Parker, D. J., Taylor, C. M., Cammas, J.-P., Bock, O., et al. (2007). Airborne observations of the impact of a convective system on the planetary boundary layer thermodynamics and aerosol distribution in the inter-tropical discontinuity region of the West African Monsoon. *Quarterly Journal of the Royal Meteorological Society*, *133*, 1175–1189
- Francis, D., Eayrs, C., Chaboureaud, J.-P., Mote, T., & Holland, D. M. (2018). Polar jet associated circulation triggered a Saharan cyclone and derived the poleward transport of the African dust generated by the cyclone. *Journal of Geophysical Research: Atmospheres*, *123*, 11899–11917. <https://doi.org/10.1029/2018JD029095>
- Francis, D., Eayrs, C., Chaboureaud, J.-P., Mote, T., & Holland, D. M. (2019). A meandering polar jet caused the development of a Saharan cyclone and the transport of dust toward Greenland. *Advances in Science and Research*, *16*, 49–56. <https://doi.org/10.5194/asr-16-49-2019>
- Francis, J. A., & Vavrus, S. J. (2012). Evidence linking Arctic amplification to extreme weather in mid-latitudes. *Geophysics Research Letters*, *39*, L06801. <https://doi.org/10.1029/2012GL051000>
- Gelaro, R., McCarty, W., Suárez, M. J., Todling, R., Molod, A., Takacs, L., et al. (2017). The Modern-Era Retrospective Analysis for Research and Applications, Version 2 (MERRA-2). *Journal of Climate*, *30*, 5419–5454. <https://doi.org/10.1175/JCLI-D-16-0758.1>
- Grob, S., Freudenthaler, V., Schepanski, K., Toledano, C., Schafner, A., Ansmann, A., & Weinzierl, B. (2015). Optical properties of long-range transported Saharan dust over Barbados as measured by dual-wavelength depolarization Raman lidar measurements. *Atmospheric Chemistry and Physics*, *15*, 11067–11080. <https://doi.org/10.5194/acp-15-11067-2015>
- Heinold, B., Knippertz, P., Marsham, J. H., Fiedler, S., Dixon, N. S., Schepanski, K., et al. (2013). The role of deep convection and nocturnal low-level jets for dust emission in summertime West Africa: Estimates from convection-permitting simulations. *Journal of Geophysical Research: Atmospheres*, *118*, 4385–4400. <https://doi.org/10.1002/jgrd.50402>
- Hsieh, J., & Cook, K. H. (2008). On the instability of the African easterly jet and the generation of African waves: Reversals of the potential vorticity gradient. *Journal of Atmospheric Science*, *65*, 2130–2151. <https://doi.org/10.1175/2007JAS2552.1>
- Kaskaoutis, D. G., Dumka, U. C., Rashki, A., Psiloglou, B. E., Gavriil, A., Mofidi, A., et al. (2019). Analysis of intense dust storms over the eastern Mediterranean in March 2018: Impact on radiative forcing and Athens air quality. *Atmospheric Environment*, *209*, 23–39. <https://doi.org/10.1016/j.atmosenv.2019.04.025>
- Kaufman, Y. J., Tanré, D., Rmer, L. A., Vermote, E. F., Chu, A., & Holben, B. N. (1997). Operational remote sensing of tropospheric aerosol over land from EOS moderate resolution imaging spectroradiometer. *Journal of Geophysical Research*, *102*, 17051–17067. <https://doi.org/10.1029/96JD03988>
- Kaufman, Y., Tanré, D., & Boucher, O. (2002). A satellite view of aerosols in the climate system. *Nature*, *419*, 215–223. <https://doi.org/10.1038/nature01091>
- Knippertz, P., Deutscher, C., Kandler, K., Müller, T., Schulz, O., & Schütz, L. (2007). Dust mobilization due to density currents in the Atlas region: Observations from the Saharan Mineral Dust Experiment 2006 field campaign. *Journal of Geophysical Research*, *112*, D21109. <https://doi.org/10.1029/2007JD008774>
- Knippertz, P. (2014). Meteorological aspects of dust storms. In P. Knippertz & J.-B. W. Stuut (Eds.), *Mineral dust* (Vol. 6, pp. 121–147). Dordrecht, The Netherlands: Springer.
- Knippertz, P., Ansmann, A., Althausen, D., Müller, D., Tesche, M., Bierwirth, E., et al. (2009). Dust mobilization and transport in the northern Sahara during SAMUM 2006 – A meteorological overview. *Tellus B: Chemical and Physical Meteorology*, *61*, 12–31. <https://doi.org/10.1111/j.1600-0889.2008.00380.x>
- Knippertz, P., & Todd, M. C. (2010). The central west Saharan dust hot spot and its relation to African easterly waves and extratropical disturbances. *Journal of Geophysical Research*, *115*, D12117. <https://doi.org/10.1029/2009JD012819>
- Knippertz, P., & Todd, M. C. (2012). Mineral dust aerosols over the Sahara: Meteorological controls on emission and transport and implications for modelling. *Reviews of Geophysics*, *50*, RG1007. <https://doi.org/10.1029/2011RG000362>
- Kornhuber, K., Osprey, S., Coumou, D., Petri, S., Petoukhov, V., Rahmstorf, S., & Gray, L. (2019). Extreme weather events in early summer 2018 connected by a recurrent hemispheric wave-7 pattern. *Environmental Research Letters*, *14*, 054002. <https://doi.org/10.1088/1748-9326-ab13b>
- Lavaysse, C., Flamant, C., Janicot, S., Parker, D. J., Lafore, J.-P., Sultan, B., & Pelon, J. (2009). Seasonal evolution of the West African heat low: A climatological perspective. *Climate Dynamics*, *33*, 313–330. <https://doi.org/10.1007/s00382-009-0553-4>
- Marsham, J. H., Parker, D. J., & Grams, C. M. (2008). Uplift of Saharan dust south of the inter-tropical discontinuity. *Journal of Geophysical Research*, *113*, D21102. <https://doi.org/10.1029/2008JD009844>
- Middleton, N.J., & Goudie, A.S. (2001). Saharan dust: Sources and trajectories. *Transactions of the Institute of British Geographers*, *26*, 165–181. <https://doi.org/10.1111/1475-5661.00013>
- Pan, B., Wang, Y., Hu, J., Lin, Y., Hsieh, J.-S., Logan, T., et al. (2018). Impacts of Saharan dust on Atlantic regional climate and implications for tropical cyclones. *Journal of Climate*, *31*, 7621–7644. <https://doi.org/10.1175/JCLI-D-16-0776.1>
- Petrie, R. E., Shaffrey, L. C., & Sutton, R. T. (2015). Atmospheric response in summer linked to recent Arctic sea ice loss. *Quarterly Journal of the Royal Meteorological Society*, *141*, 2070–2076. <https://doi.org/10.1002/qj.2502>
- Pospichal, B., Bou Karam, D., Crewell, S., Flamant, C., Hunerbein, A., Bock, O., & Said, F. (2010). Diurnal cycle of the intertropical discontinuity over West Africa analysed by remote sensing and mesoscale modelling. *Quarterly Journal of the Royal Meteorological Society*, *136*, 92–106. <https://doi.org/10.1002/qj.435>
- Prospero, J. M., & Lamb, P. J. (2003). African droughts and dust transport to the Caribbean: Climate change. *Science*, *302*(5647), 1024–1027.
- Rodriguez, S., Cuevas, E., Prospero, J. M., Alastuey, A., Querol, X., Lopez-Solano, J., et al. (2015). Modulation of Saharan dust export by the North African dipole. *Atmospheric Chemistry and Physics*, *15*, 7471–7486. <https://doi.org/10.5194/acp-15-7471-2015>
- Saha, S., Moorthi, S., Pan, H.-L., Wu, X., Wang, J., Nadiga, S., et al. (2010). The NCEP climate forecast system reanalysis. *Bulletin of the American Meteorological Society*, *91*, 1015–1057. <https://doi.org/10.1175/2010BAMS3001.1>
- Schepanski, K. (2008). Transport of mineral dust and its impact on climate. *Geosciences*, *8*, 151. <https://doi.org/10.3390/geosciences8050151>
- Schepanski, K., Heinold, B., & Tegen, I. (2017). Haramattan, Saharan heat low, and West African monsoon circulation: Modulations on the Saharan dust outflows towards the North Atlantic. *Atmospheric Chemistry and Physics*, *17*, 10223–10243. <https://doi.org/10.5194/acp-17-10223-2017>
- Schepanski, K., Tegen, I., Todd, M. C., Heinold, B., Bonisch, H., Laurent, B., & Macke, A. (2009). Meteorological processes forcing Saharan dust emission inferred from MSG-SEVIRI observations of subdaily dust source activation and numerical models. *Journal of Geophysical Research*, *114*, D10201. <https://doi.org/10.1029/2008JD010325>
- Schmetz, J., Pili, P., Tjemkes, S., Just, D., Kerkmann, J., Rota, S., & Ratier, A. (2002). An introduction to Meteosat Second Generation (MSG). *Bulletin of the American Meteorological Society*, *83*, 977–992. [https://doi.org/10.1175/1520-0477\(2002\)083<0977:AITMSG>2.3.CO;2](https://doi.org/10.1175/1520-0477(2002)083<0977:AITMSG>2.3.CO;2)

- Solomos, S., Kalivitis, N., Mihalopoulos, N., Amiridis, V., Kouvarakis, G., Gkikas, A., et al. (2018). From tropospheric folding to Kham-sin and Foehn winds: How atmospheric dynamics advanced a record-breaking dust episode in Crete. *Atmosphere*, 9, 240. <https://doi.org/10.3390/atmos9070240>
- Takaya, K., & Nakamura, H. (2001). A formulation of a phase-independent wave-activity flux of stationary and migratory Quasi-Geostrophic eddies on a zonally varying basic flow. *Journal of Atmospheric Sciences*, 58, 608–627. [https://doi.org/10.1175/1520-0469\(2001\)058<0608:AFOAPI>2.0.CO;2](https://doi.org/10.1175/1520-0469(2001)058<0608:AFOAPI>2.0.CO;2)
- Terink, W., Immerzeel, W. M., & Droogers, P. (2013). Climate change projections of precipitation and reference evapotranspiration for the Middle East and Northern Africa until 2050. *International Journal of Climatology*, 33, 3055–3072. <https://doi.org/10.1002/joc.3650>
- Thorncroft, C.D., & Blackburn, M. (1999). Maintenance of the African easterly jet. *Quarterly Journal of the Royal Meteorological Society*, 125, 763–786. <https://doi.org/10.1002/qj.49712555502>
- Tulet, P., Mallet, M., Pont, V., Pelon, J., & Boone, A. (2008). The 7–13 March 2006 dust storm over West Africa: Generation, transport, and vertical stratification. *Journal of Geophysical Research*, 113, D00C08. <https://doi.org/10.1029/2008JD009871>
- von Engel, A., & Teixeira, J. (2013). A planetary boundary layer height climatology derived from ECMWF reanalysis data. *Journal of Climate*, 26, 6575–6590. <https://doi.org/10.1175/JCLI-D-12-00385.1>
- Winker, D. M., Pelon, J. R., & McCormick, M. P. (2003). The CALIPSO mission: Spaceborne lidar for observation of aerosols and clouds. Proceedings Volume 4893, Lidar Remote Sensing for Industry and Environment Monitoring III. <https://doi.org/10.1117/12.466539>
- Weston, M. J., Temimi, M., Nelli, N. R., Fonseca, R. M., Thota, M. S., & Valappil, V. K. (2020). On the analysis of the low-level double temperature inversion over the United Arab Emirates: A case study during April 2019. *IEEE Geoscience and Remote Sensing Letters*, 1–5. <https://doi.org/10.1109/LGRS.2020.2972597>
- Xie, S.-P., Hu, K., Hafner, J., Tolinaga, H., Du, Y., Huang, G., & Sampe, T. (2009). Indian Ocean capacitor effect on Indo-Western Pacific climate during the summer following El Niño. *Journal of Climate*, 22, 730–747. <https://doi.org/10.1175/2008JCLI2544.1>